Research Article

Nano Research
2019, 12(10): 2554–2558

ISSN 1998-0124 CN 11-5974/O4
https://doi.org/10.1007/s12274-019-2484-7

Macroscopic Ag nanostructure array patterns with high-density hot-spots for reliable and ultra-sensitive SERS substrates

Taeksu Lee, Soongeun Kwon, Sanghee Jung, Hyungjun Lim, and Jae-Jong Lee (✉)

Department of Nano Manufacturing Technology, Korea Institute of Machinery and Materials (KIMM), 156 Gajeongbuk-Ro, Yuseong-Gu, Daejeon 34103, Republic of Korea

Received: 24 January 2019 / **Revised:** 16 July 2019 / **Accepted:** 18 July 2019

ABSTRACT

Synthesis of metal nanostructures arrays with large amounts of small nano-gaps on a homogenous macroscale is of significant interest and importance in chemistry, biotechnology, physics, and nanotechnology because of their enhanced properties. However, the fabrication of uncovered nano-gaps with high-density and uniformity is rather difficult due to the complex and multiple synthetic steps. In this research, a facile and low-cost approach is demonstrated for the synthesis of high-density small nano-gaps (about 3.4 nm) between silver nanostructure array patterns (SNAPs) over a large area. Uniform nano-hole patterns were periodically generated over an entire substrate using nano-imprint lithography. Electrochemical reaction at the high over-potential produced multiple silver nanocrystals inside the nano-hole patterns, generating a high-density of small and uncovered nano-gaps. Finally, we fully demonstrate their application in the rapid detection of rhodamine 6G (R6G) molecules by surface-enhanced Raman scattering (SERS) spectroscopy with a very low detection limit (1 fM) as well as excellent signal uniformity (RSD < 8.0% ± 2.5%), indicating an extraordinary capability for single-molecule detection.

KEYWORDS

nanoImprint lithography, surface-enhanced Raman scattering (SERS) spectroscopy, electrodeposition, nano patterning, gold, silver

1 Introduction

The fabrication of metal nanostructures in an array configuration with small nano-gaps on a homogenous macroscale has been highlighted in the fields of optics and metamaterials. It's because such super-structures can strongly concentrate an incident electromagnetic field into a narrow space, giving strong field localization from the plasmonic couplings between themselves, compared to single elements. Therefore, they can satisfy the practical requirements in surface enhanced Raman scattering (SERS) spectroscopy, localized surface plasmon resonance (LSPR) sensing, photovoltaics, photocatalysis, metamaterials, solar cell and so forth [1–7].

Among the various techniques to fabricate these nanostructure arrays, wet chemical based techniques, like urchin shaped alloy nanoparticles [8], vertically aligned gold nanorod arrays [9, 10], gold nanoparticle monolayer obtained by phase-transfer [4, 11], or the assembly of plasmonic nanoparticles using DNA molecules [3] have been successfully applied to generate nano-gaps and detect target molecules with highly enhanced sensitivity and specifity by SERS sensing. However, these methods are hard to be utilized in practical applications owing to structural instability and poor reproducibility as well as their unsuitability for large-scale production. To overcome these limitations, lithographic approaches, such as e-beam lithography [12], optical lithography [13, 14], atomic layer deposition [15, 16] and nanosphere lithography [17] are used to synthesize highly uniform and reliable nanostructure patterns. Unfortunately, most of these methods are quite costly and have limitations to create small nano-gaps (hot-spots) with high density.

Recently, combinations of lithographic and wet chemical strategies (nanorod bundle structure [18], antenna bowtie structures [3], and the addition of nanoparticles on patterned substrate [19, 20], etc.) have been devised and accomplished to synthesize small nano-gaps over a large area. However, these methods still require multiple complex synthesis steps and the density of the produced nano-gaps is low. Thus, to make SERS sensing a more attractive and competent technique than conventional analytical tools, the synthetic procedure should be simplified and the number of nano-gaps should be increased while ensuring that the narrow nano-gap distance is preserved [21].

Herein, we propose a simple and efficient technology to create silver nanostructure array patterns (SNAPs) with high-density nano-gaps over a large area (3 cm × 3 cm) by taking advantage of nano-imprint lithography (NIL) technique [22] and electro-deposition [23]. NIL generates uniform nano-hole patterns (NHPs) over the entire substrates and applying high over-potential (−3 V vs. Ag/AgCl) creates abundant silver nanostructure arrays inside every hole-pattern for hot-spot generation. To manifest the potential application of SNAPs in sensing fields, rhodamine 6G (R6G) detection via surface Raman enhancement spectroscopy is performed. The uniform and high density nano-gaps (about 3.4 nm) over the entire substrates produced the conditions necessary to obtain an enormously high SERS enhancement factor (1.72×10^{10}) with excellent signal uniformity (relative standard deviation (RSD) < 8.0% ± 2.5%). A well-packed assembly of silver nanostructures inside the NHPs ensures the high accessibility of the built-in hotspots by avoiding the use of a conventional organic capping agent. Moreover it provides enough binding sites for the capture of target molecules in the hot spots.

Address correspondence to jjlee@kimm.re.kr

2 Experimental

2.1 Preparation of the NHP

To prepare the NHP, Si (100) wafer was covered by 50 nm Au thin film using E-beam evaporation. Then, about 150 nm of polymethylglutarimide (PMGI) (PMGI SF5, MicroChem Corp., USA) was first spin-coated on the substrate and spin-coating of 100 nm thermal nanoimprint resist (mr-I 8010R, micro-resist technology GmbH, Germany) was followed. The bilayer resist stack was subjected to thermal nanoimprinting at 200 °C under a pressure of 70 bar for 200 s with a commercial tool (ANT-6HO3, KIMM, Republic of Korea) with the pillar patterned silicon stamp (480 nm diameter, 1,000 nm pitch), as the nanoimprint mold. After the nanoimprinting step, the residual nanoimprint resist was etched by O_2 plasma. Then, the PMGI resist was wet-etched by a commercial developer solution (AZ MIF300, AZ Electronic Materials, USA) for 3 s.

2.2 Synthesis and characterization of the SNAPs substrates

Prior to the electrodeposition process, the non-reactive area on the substrates was passivated by lacquer for better fixation of the substrates on the working electrode and determining the reactive area for the silver nanostructure growth in the NHP. We performed the electrochemical experiments with the conventional three-electrode system (Pt counter electrode and an Ag/AgCl (3 M KCl) reference electrode) thorough a potentiostat (CompactStat, Ivium). A 2 mM silver-plating solution was prepared, and the pH was controlled using sodium carbonate. To determine the most appropriate degree of over-potential, SNAPs were prepared at over-potentials ranging from −1.0 to −3.0 V (vs. Ag/AgCl electrode as a reference electrode) at room temperature using the NHPs prepared. Then, the polymer resist was removed with an excess amount of acetone (OCI, Republic of Korea) and AZ-MIF 300 developer. The morphology the SNAPs was analyzed by field emission scanning electron microscopy (FE-SEM) (S-4800, Hitachi, Japan). The nano-gap distribution and the number of nano-gaps in the synthesized substrates, from each synthetic condition, were measured by analyzing SEM images with the ImageJ program. For a more sophisticated analysis, we adjusted the brightness and saturation in the SEM images. When we counted the number of nano-gaps, we considered the gaps only when two neighboring nanostructures were close enough and we defined the nano-gaps as the shortest distance between the neighboring two silver nanostructures. The crystal structures of the NHP and SNAPs were investigated by X-ray diffraction analysis (PANalytical B.V., the Netherlands) at room temperature. The surface elements in the NHP and SNAPs were measured using an X-ray photoelectron spectrometer (K-alpha, Thermo, UK) with a monochromatic Al Kα X-ray source.

2.3 SERS measurements

Prior to the Raman analysis, solutions of R6G (10^{-15} to 10^{-8} and 10^{-3} M) and p-aminothiophenol (p-ATP, 10^{-6} M), in ethanol, were prepared. At first, 479.02 mg of R6G and 125.19 mg of p-ATP were dissolved in 10 mL of ethanol, separately. Different concentration of dye solutions was prepared by serial 10-fold dilutions of the samples. The fabricated substrates were immersed in each solution for 4 h and dried in the oven for few minutes. Raman spectroscopy measurements were performed with a confocal Raman microscope (Renishaw inVia Raman Microscope). The laser power on the sample was approximately 1 mW, and the integration time was 10 s. A silicon wafer with a Raman band at 520 cm^{-1} was used as the reference for calibration. Wire 3.2 software was used for spectral and image processing and analysis. For demonstrating the stability of fabricated substrates, we prepared two kinds of SNAPs. We treated 10^{-6} M of p-ATP right after SNAPs fabrication, and the 10^{-6} M of p-ATP solution was added after 10 days of SNAPs synthesis. The synthesized SNAPs were preserved in the desiccator and at room temperature, in order to prevent the possible oxidation. Both p-ATP and R6G were purchased from Sigma-Aldrich, Republic of Korea.

2.4 Calculation of SERS enhancement factor

The analytical SERS enhancement factors (EFs) for R6G molecules on the SNAPs, were estimated, using the following expression

$$EF = (I_{SNAPs}/I_{dye}) \times (C_{dye}/C_{SNAPs}) \quad (1)$$

where C_{dye} and C_{SNAPs} represent the concentration of R6G molecules on the bare Si substrate (after 10^{-3} M R6G solution-treated) and the number of R6G molecules on the surface of SNAPs (after 10^{-13} M R6G solution-treated), respectively; I_{dye} and I_{SNAPs} are the signal intensities of the R6G Raman spectra on the pure Si substrate (after 10^{-3} M R6G solution-treated) and on the surface of SNAPs (after 10^{-13} M R6G solution-treated), respectively.

3 Results and discussion

Our fabrication technique involves nano-imprint lithography on a substrate, which can create uniform polymer cavity arrays over the entire substrate, and generation of plenty of silver nanostructures inside the hole-patterns (Scheme 1). First, as a substrate for generating SNAPs, uniform NHPs were prepared via the nano-imprint lithography method (Fig. S1 in the Electronic Supplementary Material (ESM)). When we applied over-potential to the substrates, all the NHPs were deposited with silver nanostructures (Fig. 1, and Figs. S2 and S3 in the ESM). The thermal nanoimprint resist and PMGI were removed with excess amount of acetone and AZ-MIF300, respectively. The silver nanostructures were deposited only inside the NHPs. Because the outside of the nano-holes were blocked by the non-conductive thermal nanoimprint resist and PMGI, only the bottom of the nano-holes was opened to the silver precursors. Therefore, the seeds for nanostructure fabrication were only generated at the bottom of the nano-holes [1]. The granular size of each silver nanostructures was diminished with respect to the over-potential values since further over-potential increment resulted in an enhanced current, leading to the formation of multiple silver seeds at the initial stage. Especially, when the −3 V of over-potential was applied, the rapid growth of multiple silver nanostructures resulted in the generation of multitudes of small nano-gaps between the silver nanostructures. The average gap size significantly decreased to 3.4 nm (Figs. S5 and S6 in the ESM), while the number of nano-gaps per unit area increased to 132 nano-gaps/μm^2 (Fig. 2). The height of

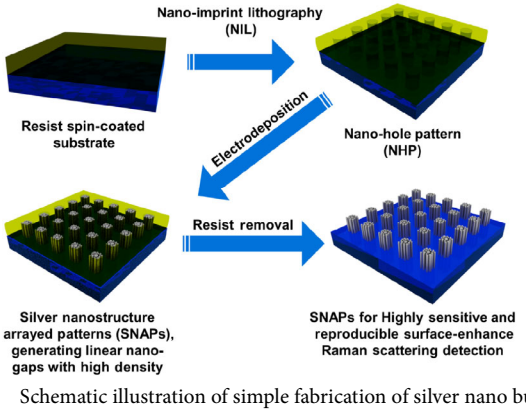

Scheme 1 Schematic illustration of simple fabrication of silver nano bundles in the nano-hole patterns. At first, uniform nano-hole patterns were fabricated via the nano-imprint lithography method. Silver nano-bundles were electrodeposited in the hole-patterns and generated small, nano-gaps (around 3.4 nm) with high density. At last, the resist polymer was removed with excess amounts acetone and a basic developer for ultra-sensitive and robust SERS detection.

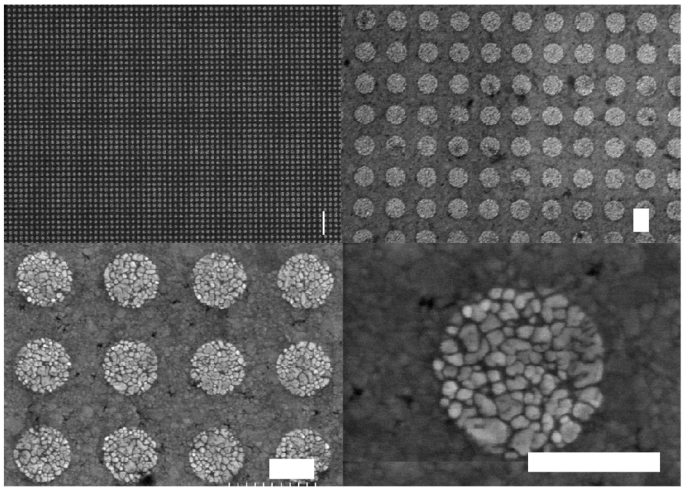

Figure 1 Representative SEM images of SNAPs. The scale bar represents 500 nm.

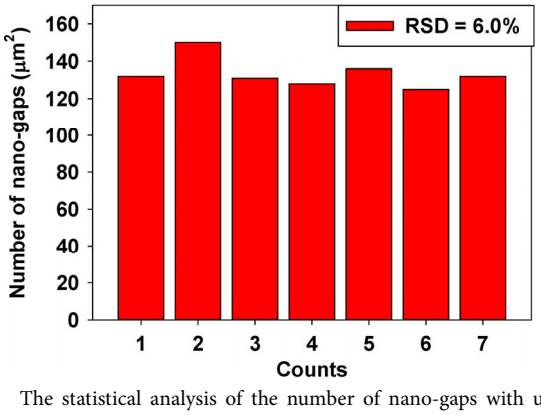

Figure 2 The statistical analysis of the number of nano-gaps with unit area (1 μm^2) at different positions of SNAPs.

the SNAPs was about 150 nm because the growth of SNAPs was confined by the PMGI and thermal resist, as shown in Fig. S4 in the ESM. When we calculated the number of hot-spots, nano-gaps larger than 10 nm were excluded because of their low contribution to the SERS performance [4]. The RSD value of nano-gap density was about 6.0%, which clearly showed the reproducibility of our substrates. Hence, we performed the further experiments under –3 V over-potential appliance.

Having observed the successful synthesis of numerous 3.4 nm nano-gaps over a large area, we next conducted the X-ray diffraction studies and confirmed that the SNAPs were highly crystalline (Fig. 3(a)) [23, 24]. The surface chemical compositions of the SNAPs demonstrate a successful silver deposition. Figures 3(b) and 3(c) show the spectra of the Au 4f and Ag 3d orbitals in high resolution. NHPs present two dominating gold signals (87.4 and 83.7 eV) matching for the Au $4f_{5/2}$ and Au $4f_{7/2}$ orbitals. The difference in binding energy between the doublet peaks is 3.7 eV with a 4:3 intensity ratio, and can be indexed to Au^0. In contrast, SNAPs shows the doublet peaks of Ag $3d_{3/2}$ and $3d_{5/2}$, centered at 373 and 367 eV. The energy difference between the two peaks is 6.0 eV and the intensity ratio of these doublet peaks is 2:3, demonstrating the appearance of silver in its zero-valent form Ag^0 in the system [25]. We can manifest the successful silver deposition onto NHPs from these X-ray photoelectron spectroscopy results, supporting the conclusion that the SERS enhancement of the nanostructures was based on the surface silver composition.

After structural chemical analysis of the SNAPs, the plasmonic properties of the SNAPs were determined in SERS analysis, on a commercial Raman spectrometer with 633 nm laser excitation. It is envisaged that periodically uniform silver nanorod arrays with consistent nano-gap size and distribution can produce reproducible SERS signal. Previously, SERS substrates have been often suffered from signal inconsistency, which has been a big hurdle for SERS substrates to be utilized in practical applications. To demonstrate the high SERS uniformity of SNAPs, we measured the SERS spectra taken from more than 50 randomly selected points after 10^{-6} M p-ATP dye treatment (Fig. 4). The intensities of the characteristic vibration at 1,078 (C–C stretching and C–S stretching), 1142 (C–N stretching mode) and 1,578 (parallel C–C stretching vibration) cm^{-1} are shown in Fig. 4(a). In these spectra, the N=N stretching vibration peak mode at 1,434 cm^{-1} indicates that the p-ATP consists 4,4'-dimercaptoazobenzene (DMAB) at this treated concentration [26]. The mapping image supports the reproducibility of the SERS signals (Fig. 4(b)). In order to analyze the signal uniformity specifically, the RSD of the intensities at 1,078, 1,142 and 1,578 cm^{-1} are analyzed to be only 7.2%, 8.5% and 8.3%, respectively, and the average RSD value is 8.0%, demonstrating high signal uniformity of the ordered SNAPs (Fig. 4(c)). It should be emphasized that these regions of interest were randomly selected and that consistent spatial uniformity could be found over the entire SERS substrate.

The intensities of the Raman peaks of p-ATP (1,078, 1,141, 1,391, 1,435 and 1,578 cm^{-1}) at the SNAPs were retained after 10 days of fabrication (Fig. S9 in the ESM). Based on this result, we confirmed the presented SNAPs had good signal stability within 10 days, indicating the feasibility of actual field applications.

In addition to high uniformity and reproducibility, the SNAPs also showed excellent SERS EF value of 1.72×10^{10}, calculated with R6G as a probe molecule (Fig. S10 in the ESM). This notable EF increment in the SNAPs is ascribed to two distinct factors, namely: large amounts of well-designed nano-gaps between the silver nanostructures; and the silver surface composition, which has an inherently higher SERS intensity than that of gold [27]. SERS is a type of surface spectroscopy, which means that only the adsorbed molecules contribute to the signal and that the effect is distance-dependent. It implies that increased dye molecule concentration can induce the multilayer deposition of dye molecules onto the SERS substrate, which hinders the exact calculation of EF values. Therefore, we chose

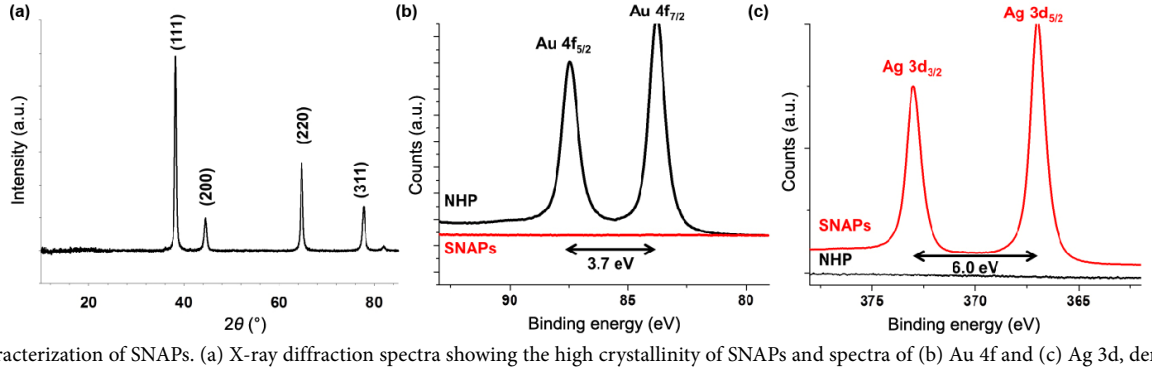

Figure 3 Characterization of SNAPs. (a) X-ray diffraction spectra showing the high crystallinity of SNAPs and spectra of (b) Au 4f and (c) Ag 3d, demonstrating the successful silver deposition on the hole patterns.

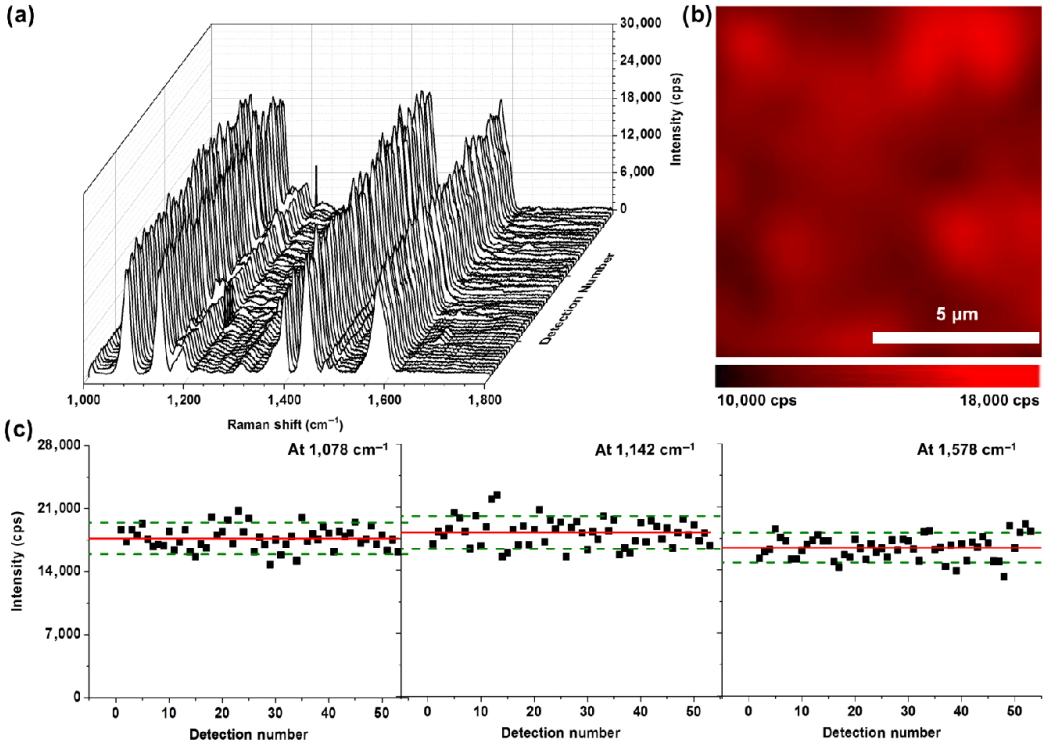

Figure 4 Uniformity of the SNAPs. (a) SERS spectra recorded from more than 50 random positions after 10^{-6} M of p-ATP treatment. (b) Raman mapping covering 20 μm × 20 μm showing the intensity of the Raman signal band around 1,578 cm^{-1}, as a function of coordinates. (c) Intensity deviation of 1,078, 1,142 and 1,578 cm^{-1} peaks from (a). Red line represents the average intensity and the green dotted line shows ±10% standard deviation.

the 10^{-12} M concentration, the lowest and detectable dye concentration to optimize that one monolayer of R6G absorbed on SNAPs [28].

To further explore the applications of SNAPs in the sensing field, the as-prepared SERS substrate was used to detect R6G, as a probe molecule, in ethanol and the SERS intensities of three different Raman shifts at 1,360, 1,508 and 1,648 cm^{-1} as a function of R6G concentration (1×10^{-15}–1×10^{-8} M) are plotted in Fig. 5. The results demonstrate that the Raman intensities of the R6G in the SNAPs decreased as the loaded R6G concentration decreased. We defined the limit of detection (LOD) as the concentration at which the signal to noise ratio is equal to 4. Based on this criteria, the distinct Raman peaks of R6G at 1,360, 1,508 and 1,648 cm^{-1} could still be clearly distinguishable, even when the concentration of R6G was as low as 10^{-15} M, without any aid of the SERS effect. This notable LOD enhancement is attributed to the combination of the joint electromagnetic (EM) field enhancement and the large number of binding sites in SNAPs. The synthesized SNAPs have also good linear calibration curves between logarithmic R6G concentration and SERS intensities at 1,360, 1,508 and 1,648 cm^{-1} ($r^2 = 0.99$). The slopes at 1,360, 1,508 and 1,648 cm^{-1} were measured to be 0.25, 0.24 and 0.23.

4 Conclusions

We have demonstrated a facile and low-cost methodology for the synthesis of silver nano-structure arrays via nano-imprint lithography and electrodeposition. The periodical silver nano-structures facilitate strong nano-gap generation with high-density as well as evenly distributed hot-spots over the entire substrates. These unique nanostructure arrays demonstrate excellent SERS sensitivity and reproducibility. Moreover, the nano-gap arrays in SNAPs without capping agents enable easy access to the target molecules. The synthesized SNAPs could be utilized as a SERS substrate that exhibited Raman signal enhancement as high as 10^{10} with excellent uniformity and high reproducibility of the SERS signal (RSD < 8.0% ± 2.5%) and also detect R6G at a target concentration as low as 10^{-15} M. This strategy can be readily extended to the macroscopic synthesis of various metal nanostructure arrays and bridge the gap between nanoscale materials and macroscopic applications.

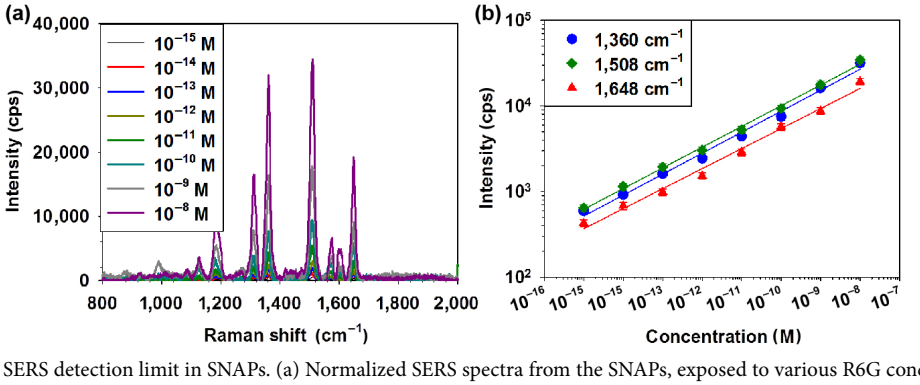

Figure 5 Examination of the SERS detection limit in SNAPs. (a) Normalized SERS spectra from the SNAPs, exposed to various R6G concentrations (10^{-15} to 10^{-8} M) under the 633 nm laser irradiation; data collection 10 s; incident laser power 1 mW. (b) Calibration curves of SERS intensity at 1,360, 1,508 and 1,648 cm^{-1} against different R6G logarithmic concentration. In order to obtain statistical data, 5 random points were collected at each concentration.

Acknowledgements

This work was supported by the BioNano Health-Guard Research Center funded by the Ministry of Science and ICT & Future Planning (MSIP) of Korea as Global Frontier Project (No. H-GUARD_2013M3A6B2078) and the Nano-Material Technology Development Program of the National Research Foundation (NRF) funded by the Ministry of Science and ICT (No. 2017M3A7B4041754).

Electronic Supplementary Material: Supplementary material (further details of SEM images, nanogap distribution measurements and Raman spectroscopy measurements) is available in the online version of this article at https://doi.org/10.1007/s12274-019-2484-7.

References

[1] Lee, T.; Wi, J. S.; Oh, A.; Na, H. K.; Lee, J.; Lee, K.; Lee, T. G.; Haam, S. Highly robust, uniform and ultra-sensitive surface-enhanced Raman scattering substrates for microRNA detection fabricated by using silver nanostructures grown in gold nanobowls. *Nanoscale* **2018**, *10*, 3680–3687.

[2] Wu, K. Y.; Li, T.; Schmidt, M. S.; Rindzevicius, T.; Boisen, A.; Ndoni, S. Gold nanoparticles sliding on recyclable nanohoodoos—Engineered for surface-enhanced Raman spectroscopy. *Adv. Funct. Mater.* **2018**, *28*, 1704818.

[3] Zhan, P. F.; Wen, T.; Wang, Z. G.; He, Y. B.; Shi, J.; Wang, T.; Liu, X. F.; Lu, G. W.; Ding, B. Q. DNA origami directed assembly of gold bowtie nanoantennas for single-molecule surface-enhanced Raman scattering. *Angew. Chem., Int. Ed.* **2018**, *57*, 2846–2850.

[4] Si, S. R.; Liang, W. K.; Sun, Y. H.; Huang, J.; Ma, W. L.; Liang, Z. Q.; Bao, Q. L.; Jiang, L. Facile fabrication of high-density sub-1-nm gaps from Au nanoparticle monolayers as reproducible SERS substrates. *Adv. Funct. Mater.* **2016**, *26*, 8137–8145.

[5] Kurouski, D.; Mattei, M.; Van Duyne, R. P. Probing redox reactions at the nanoscale with electrochemical tip-enhanced Raman spectroscopy. *Nano Lett.* **2015**, *15*, 7956–7962.

[6] Park, K. D.; Muller, E. A.; Kravtsov, V.; Sass, P. M.; Dreyer, J.; Atkin, J. M.; Raschke, M. B. Variable-temperature tip-enhanced Raman spectroscopy of single-molecule fluctuations and dynamics. *Nano Lett.* **2016**, *16*, 479–487.

[7] Lee, T.; Jung, S.; Kwon, S.; Kim, W.; Park, J.; Lim, H.; Lee, J. Formation of interstitial hot-spots using the reduced gap-size between plasmonic microbeads pattern for surface-enhanced Raman scattering analysis. *Sensors* **2019**, *19*, 1046.

[8] Liu, Z.; Yang, Z. B; Peng, B.; Cao, C.; Zhang, C.; You, H. J.; Xiong, Q. H.; Li, Z. Y.; Fang, J. X. Highly sensitive, uniform, and reproducible surface-enhanced Raman spectroscopy from hollow Au-Ag alloy nanourchins. *Adv. Mater.* **2014**, *26*, 2431–2439.

[9] Thai, T.; Zheng, Y. H.; Ng, S. H.; Mudie, S.; Altissimo, M.; Bach, U. Self-assembly of vertically aligned gold nanorod arrays on patterned substrates. *Angew. Chem., Int. Ed.* **2012**, *51*, 8732–8735.

[10] Li, P. H.; Li, Y.; Zhou, Z. K.; Tang, S. Y.; Yu, X. F.; Xiao, S.; Wu, Z. Z.; Xiao, Q. L.; Zhao, Y. T.; Wang, H. Y. et al. Evaporative self-assembly of gold nanorods into macroscopic 3D plasmonic superlattice arrays. *Adv. Mater.* **2016**, *28*, 2511–2517.

[11] Shin, Y.; Song, J.; Kim, D.; Kang, T. Facile preparation of ultrasmall void metallic nanogap from self-assembled gold-silica core-shell nanoparticles monolayer via kinetic control. *Adv. Mater.* **2015**, *27*, 4344–4350.

[12] Lin, Q. Y.; Li, Z. Y.; Brown, K. A.; O'Brien, M. N.; Ross, M. B.; Zhou, Y.; Butun, S.; Chen, P. C.; Schatz, G. C.; Dravid, V. P. et al. Strong coupling between plasmonic gap modes and photonic lattice modes in DNA-assembled gold nanocube arrays. *Nano Lett.* **2015**, *15*, 4699–4703.

[13] Lim, H.; Ryu, J.; Kim, G.; Choi, K. B.; Lee, S.; Lee, J. Nanoimprint lithography with a focused laser beam for the fabrication of nanopatterned microchannel molds. *Lab Chip* **2013**, *13*, 3188–3191.

[14] Ahn, J.; Kwon, S.; Jung, S.; Lee, W. S.; Jeong, J.; Lim, H.; Shin, Y. B.; Lee, J. Fabrication of pyrrole-based electrochemical biosensor platform using nanoimprint lithography. *Adv. Mater. Interfaces* **2018**, *5*, 1701593.

[15] Yoon, J. K.; Nam, S.; Shim, H. C.; Park, K.; Yoon, T.; Park, H. S.; Hyun, S. Highly-stable $Li_4Ti_5O_{12}$ anodes obtained by atomic-layer-deposited Al_2O_3. *Materials* **2018**, *11*, 803.

[16] Zhang, X. Y.; Zhao, J.; Whitney, A. V.; Elam, J. W.; Van Duyne, R. P. Ultrastable substrates for surface-enhanced Raman spectroscopy: Al_2O_3 overlayers fabricated by atomic layer deposition yield improved anthrax biomarker detection. *J. Am. Chem. Soc.* **2006**, *128*, 10304–10309.

[17] Lee, J.; Zhang, Q. P.; Park, S.; Choe, A.; Fan, Z. Y.; Ko, H. Particle-film plasmons on periodic silver film over nanosphere (AgFON): A hybrid plasmonic nanoarchitecture for surface-enhanced Raman spectroscopy. *ACS Appl. Mater. Interfaces* **2016**, *8*, 634–642.

[18] Zhu, C. H.; Meng, G. W.; Zheng, P.; Huang, Q.; Li, Z. B.; Hu, X. Y.; Wang, X. J.; Huang, Z. L.; Li, F. D.; Wu, N. Q. A hierarchically ordered array of silver-nanorod bundles for surface-enhanced Raman scattering detection of phenolic pollutants. *Adv. Mater.* **2016**, *28*, 4871–4876.

[19] Li, X. L.; Zhang, Y. Z.; Shen, Z. X.; Fan, H. J. Highly ordered arrays of particle-in-bowl plasmonic nanostructures for surface-enhanced Raman scattering. *Small* **2012**, *8*, 2548–2554.

[20] Li, X. M.; Bi, M. H.; Cui, L.; Zhou, Y. Z.; Du, X. W.; Qiao, S. Z.; Yang, J. 3D aluminum hybrid plasmonic nanostructures with large areas of dense hot spots and long-term stability. *Adv. Funct. Mater.* **2017**, *27*, 1605703.

[21] Zhang, L.; Guan, C. R.; Wang, Y.; Liao, J. H. Highly effective and uniform SERS substrates fabricated by etching multi-layered gold nanoparticle arrays. *Nanoscale* **2016**, *8*, 5928–5937.

[22] Kim, Y.; Kim, G.; Lee, J. Fabrication of a conductive nanoscale electrode for functional devices using nanoimprint lithography with printable metallic nanoink. *Microelectron. Eng.* **2010**, *87*, 839–842.

[23] Bang, D.; Chang, Y. W.; Park, J.; Lee, T.; Park, J.; Yeo, J. S.; Kim, E. K.; Yoo, K. H.; Huh, Y. M.; Haam, S. One-step electrochemical fabrication of vertically self-organized silver nanograss. *J. Mater. Chem. A* **2013**, *1*, 4851–4857.

[24] Lee, T.; Bang, D.; Chang, Y. W.; Choi, Y.; Park, K. Y.; Oh, A.; Han, S.; Kim, S. H.; Lee, K.; Suh, J. S. et al. Cancer theranosis using mono-disperse, mesoporous gold nanoparticles obtained via a robust, high-yield synthetic methodology. *RSC Adv.* **2016**, *6*, 13554–13561.

[25] Liu, Y. J.; Pedireddy, S.; Lee, Y. H.; Hegde, R. S.; Tjiu, W. W.; Cui, Y.; Ling, X. Y. Precision synthesis: designing hot spots over hot spots via selective gold deposition on silver octahedra edges. *Small* **2014**, *10*, 4940–4950.

[26] Park, J.; Bang, D.; Jang, K.; Kim, E.; Haam, S.; Na, S. Multimodal label-free detection and discrimination for small molecules using a nanoporous resonator. *Nat. Commun.* **2014**, *5*, 3456.

[27] Sivasubramanian, R.; Sangaranarayanan, M. V. Electrodeposition of silver nanostructures: From polygons to dendrites. *CrystEngComm* **2013**, *15*, 2052–2056.

[28] Le Ru, E. C.; Blackie, E.; Meyer, M.; Etchegoin, P. G. Surface enhanced Raman scattering enhancement factors: A comprehensive study. *J. Phys. Chem. C* **2007**, *111*, 13794–13803.